ADVANCED THEORY AND SIMULATIONS
www.advtheorysimul.com

Comparative Analysis of Excitonic and Biexcitonic Effects on the Power Conversion Efficiency of a CdSe/CdTe/ZnTe Quantum Dot Solar Cell

*Murat Unluler and Fatih Koc**

In this study, the power conversion efficiency (PCE) of a CdSe/CdTe/ZnTe quantum dot solar cell (QDSC) is investigated considering the influence of internal parameters such as CdSe core radius and CdTe and ZnTe shell thickness along with external parameters such as temperature and hydrostatic pressure. A comparative analysis is performed using both the original detailed balance model (ODBM) and the modified detailed balance model (MDBM). The main focus of the research is to investigate the effects of excitonic and biexcitonic effective gap energies, as well as the biexciton bound state, on the PCE in the presence of multiple exciton generation (MEG). Calculations using both ODBM and MDBM indicate that the distinct excitonic and biexcitonic effective bandgap energies, resulting from strong confinement effects in quantum dot (QD) structures, significantly affect the PCE in the presence of MEG. In addition, MDBM calculations considering the biexciton bound state show that this bound state critically affects the PCE. The discrepancy between the theoretically predicted maximum PCE and the considerably lower PCE observed in practical applications of QDSCs is also examined, along with the potential reasons for this phenomenon.

1. Introduction

Quantum dot solar cells (QDSCs) have bandgap energies that depend on the size and material of the quantum dots.[1] This characteristic enables for the implementation of a cost-effective solution that effectively captures a broader range of the solar spectrum in comparison to multi-junction solar cells.[2,3] Furthermore, the process of MEG, which is crucial for classifying QDSCs as next-generation photovoltaics, plays a pivotal role in achieving higher PCE than that of conventional solar cell technologies.[4–6] MEG entails the excitation of multiple electron–hole pairs from a single photon with an energy exceeding the bandgap, thereby enhancing the overall current contribution.[7] These advantages make QDSCs a promising technology for the future of solar energy, with the potential to exceed the Shockley–Queisser limit[8] of 33% for single-junction solar cells. Research on these structures has continued to increase in recent years.[9–14]

In order to achieve the greatest possible PCE in a solar cell, it is essential that the bandgap energy of the semiconductor material is optimized to an ideal value. For single-junction solar cells, the optimal bandgap energy is estimated to be approximately 1.3 eV,[15] as predicted by the Shockley–Queisser (SQ) model. However, when MEG is taken into account, the optimal bandgap is observed to shift to approximately 0.8 eV.[16] Quantum dot (QD) structures are optimal candidates for attaining these ideal gap energies, given their tunable size and material properties. However, these structures can also give rise to processes that have a detrimental effect on PCE, such as Auger recombination and phonon interactions.[17,18] For example, as the size of the quantum dot decreases, the overlap of electron–hole wave functions increases, which results in a more dominant Auger process. Conversely, as the size increases, the quantized energy levels become closer together, which enhances the influence of phonon interactions. Moreover, alterations in the sizes of quantum dots can significantly impact the recombination processes occurring within these structures. As an illustration, an increased overlap between electron–hole wave functions results in an enhanced electron-hole recombination rate (decreased carrier lifetime), which has a negative impact on the PCE of the device. The susceptibility of QDSCs to these variables in their electronic and optical properties highlights the necessity for further research. Given that the current practical maximum PCE for QDSCs is approximately 19.1%,[19] it is evident that these structures are still operating significantly below their theoretically calculated maximum potential, emphasizing the need for continued investigation.

The electronic and optical properties of quantum dot structures are also subject to influence from the confinement regime. In core/shell structures, where both electrons and holes are confined within the same material, they are classified as type-I

M. Unluler
Department of Advanced Technologies
Ahi Evran University
Kırşehir 40100, Turkey
F. Koc
Department of Metallurgical and Materials Engineering
Ahi Evran University
Kırşehir 40100, Turkey
E-mail: f.koc@ahievran.edu.tr

The ORCID identification number(s) for the author(s) of this article can be found under https://doi.org/10.1002/adts.202400956

DOI: 10.1002/adts.202400956

structures. In contrast, type-II structures comprise electrons and holes that are localized in different materials. Type-I structures are renowned for their higher quantum efficiency, whereas type-II structures are distinguished by a lower electron-hole wave function overlap, which results in diminished oscillator strength and extended carrier lifetimes.[20] Additional structures that exhibit both type-I and type-II characteristics are the multi-shell quantum dot (onion-like quantum dots). In these structures, it is possible to form multiple potential wells for both electrons and holes.[21–23] By modifying the size of the shell layers and the confinement potential, it is possible to trap charges in specific regions. Furthermore, in multi-shell quantum dots, electrons and holes can be confined in separate materials, with a third material inserted between them. This allows for precise control over the electron–hole wave function overlap, which in turn affects the oscillator strength, a measure of the probability of electron-hole recombination.[24]

Another critical factor affecting the electronic and optical properties of quantum dot structures is the number of localized charges within QD structures. In a semiconductor quantum dot, the localization of a single electron and a single hole results in an attractive Coulomb force between them, forming a bound state known as an exciton. Conversely, if a quantum dot contains one electron and two holes, it is referred to as a positive trion; if it contains two electrons and one hole, it is referred to as a negative trion; and if it contains two electrons and two holes, it is referred to as a biexciton. As is well known, the electronic and optical properties of a quantum dot can vary significantly depending on the quasi-particles generated by optical excitation, including excitons, positive and negative trions, and biexcitons.[25–27] For example, a quantum dot of the same sizes can exhibit quite different energy levels, lifetimes, and recombination probabilities for excitons, positive and negative trions, and biexcitons.[28] In the context of QDSCs, the MEG state allows for the excitation of up to two electron–hole pairs from a single photon, forming a biexciton. Due to the attractive and repulsive Coulomb forces and exchange-correlation effects, the electronic and optical properties of biexcitons differ from those of single excitons. It can be reasonably deduced that direct gap energy-based calculations focused on exciton energy levels may not yield accurate PCE results for with MEG state. Studies have indicated that the MEG threshold varies significantly between different materials,[29–36] with values often exceeding twice the effective gap energy.[6,37,38] In light of these considerations, it can be crucial to ascertain whether excitonic or biexcitonic parameters are employed when calculating the PCE for a QDSC in the with MEG scenario. This distinction can significantly influence the accuracy of the PCE predictions.

In the field of solar cell research, the detailed balance model proposed by Shockley and Queisser[8] has become a leading tool for calculating the maximum PCE of these devices. This model serves as a foundational tool in the field, providing a methodology for calculating the maximum PCE based on the bandgap energy of the semiconductor material utilized in the solar cell. Conversely, Sahin[39] has enhanced the detailed balance model by incorporating oscillator strength, a parameter reflecting the distinct confinement regimes, recombination mechanisms, and lifetimes of QD structures, into the calculation of recombination current density. Accordingly, the MDBM can provide a PCE value specific to each structure employed in the solar cell. Given that the electronic and optical properties of QD structures can be significantly influenced by a multitude of internal and external factors, obtaining a PCE value specific to each QDSC could serve as a valuable reference for applications in this field.

This study examines the influence of the CdSe core radius, the thicknesses of the CdTe and ZnTe layers, temperature, and hydrostatic pressure on the PCE of a CdSe/CdTe/ZnTe QDSC. PCE calculations were conducted using two models: the ODBM, which considers solely the bandgap energy, and the MDBM, which additionally accounts for oscillator strength. In QD structures, the excitonic and biexcitonic effective gap energies, along with the biexciton bound state, are of greater significance than in their bulk parents. This study examines the influence of these factors on PCE, with a particular focus on their role in MEG. Furthermore, calculations using the MDBM have examined the effects of the biexciton bound state on the PCE, in addition to the calculations made with the ODBM. By examining these factors across a broad range of conditions, this study aims to provide valuable insights that can inform the design of more efficient QDSCs.

2. Model and Theory

2.1. Oscillator Strength

The MDBM is distinguished from the ODBM by its incorporation of the oscillator strength parameter into the calculation of recombination current density. This parameter, which indicates the probability of carrier recombination in QD structures, can be derived from the wave functions of the localized electron and hole within the structure. The oscillator strength is highly sensitive to both internal factors, such as size and material variations, and external conditions, such as temperature and pressure. As a result, this parameter serves as a critical metric for accurately reflecting the effects of these variables on recombination processes. For a single exciton (X), the recombination oscillator strength is calculated as follows[40]:

$$f_X = \frac{E_p}{2E_{gap}}\left|\int \psi_e(r)\psi_h(r)d^3r\right|^2 \tag{1}$$

Here, E_p is an energy related to the Kane momentum parameter, E_{gap} denotes the effective gap energy. It is important to note that the effective gap energy is the sum of the bulk gap energy, E_{gap}^{bulk}, the electron energy, E_e, and the hole energy, E_h. This can be expressed as $E_{gap} = E_{gap}^{bulk} + E_e + E_h$. ψ_e and ψ_h are the wave functions of the electron and hole, respectively. The wave functions of the electron and hole are determined by multiplication of the radial wave functions of the electron, R_e, and hole, R_h, with spherical harmonics, i.e., $\psi_{e(h)}(r) = R_{e(h)}^{n,l}(r)Y_{l,m}(\theta,\phi)$. In this study, only the ground state energy levels are examined; thus, the spherical harmonics are set to the value of $Y_{l,m}(\theta,\phi) = Y_{0,0}(\theta,\phi) = 1/\sqrt{4\pi}$. The radial wave functions R_e and R_h are obtained by solving the following Schrödinger equations self-consistently,[41]

$$\left[-\frac{\hbar^2}{2}\vec{\nabla}_r\left(\frac{1}{m_e^*(r,T,P)}\vec{\nabla}_r\right) + V_e(r,T,P) - q_e\Phi_h\right]R_e(r,T,P)$$
$$= \varepsilon_e^X(T,P)R_e^X(r,T,P) \tag{2}$$

and

$$\left[-\frac{\hbar^2}{2}\vec{\nabla}_r\left(\frac{1}{m_h^*(r,T,P)}\vec{\nabla}_r\right)+V_h(r,T,P)-q_h\Phi_e\right]R_h(r,T,P)$$
$$=\varepsilon_h^X(T,P)R_h^X(r,T,P) \quad (3)$$

Here, $m_e^*(r,T,P)$ and $m_h^*(r,T,P)$ denote the effective masses of the electron and hole, respectively, which depend on radial position, temperature, and pressure. The confinement potentials, $V_e(r,T,P)$ and $V_h(r,T,P)$, also vary with radial position, temperature, and pressure. The electrostatic potentials for the electron and hole are represented by Φ_e and Φ_h. The two aforementioned equations have been discretized using the finite difference technique and converted into a matrix eigenvalue equation. This enables the single particle energies, $\varepsilon_e(T,P)$ and $\varepsilon_h(T,P)$, and the radial wavefunctions, $R_e(r,T,P)$ and $R_h(r,T,P)$, of electrons and holes to be calculated using the matrix diagonalization technique. In this study, the eigenvalues and eigenfunctions of matrix equations have been obtained using the ALGLIB subroutine.

The effects of temperature and hydrostatic pressure are included in the calculations through the temperature- and pressure-dependent variations of the gap energy, which in turn affect the effective masses of the electrons and holes. The radial, temperature, and pressure-dependent effective masses of electrons and holes can be expressed as follows,[42]

$$m_e^*(r,T,P)=m_0\left[1+\frac{E_P}{3}\left(\frac{2}{E_g(T,P)}+\frac{1}{E_g(T,P)+\Delta_0}\right)\right]^{-1} \quad (4)$$

and

$$m_h^*(r,T,P)=m_h(r,0,0)\left(\frac{E_g(T,P)}{E_g(0,0)}\right) \quad (5)$$

where m_0 represents the free electron mass, and Δ_0 corresponds to the spin-orbit splitting energy. The values $E_g(0,0)$ and $m_h(r,0,0)$ indicate the gap energy and the effective mass of the hole at zero temperature, $T=0$ K and zero pressure, $P=0$ GPa, respectively. The gap energy $E_g(T,P)$ as a function of temperature and pressure is expressed as follows[42]:

$$E_g(T,P)=E_g(0,0)-\frac{\alpha T^2}{(T+\beta)}+aP+bP^2 \quad (6)$$

Here, α and β refer to the Varshni parameters of the materials, a and b denote the hydrostatic pressure parameters.[42]

The electrostatic Coulomb potential term, represented by the third term in Equations (2) and (3), can be obtained by solving the Poisson equation. The attractive Coulomb terms ($q_e\Phi_h$ and $q_h\Phi_e$) between the electron and hole couple the two separate Schrödinger equations into a single one. The Poisson equations, forming this coupled system, can be written as follows[43]:

$$\vec{\nabla}\kappa(r,T,P)\vec{\nabla}\Phi_e=q_e\rho_e(r,T,P), \qquad \vec{\nabla}\kappa(r,T,P)\vec{\nabla}\Phi_h=-q_h\rho_h(r,T,P) \quad (7)$$

Upon examination of the Equations (2) and (3), it becomes evident that they describe a single exciton, or a single electron-hole pair. It is, however, well established that multiple electron-hole pairs can be localized within a QD structure. A CdSe/CdTe/ZnTe QD can accommodate two electron-hole pairs, or a biexciton (XX), in its ground state. In the biexciton state, the presence of two electrons and two holes necessitates the consideration of the repulsive Coulomb potential between electrons and between holes, as well as exchange-correlation effects, in contrast to the exciton state.

The existing literature demonstrates that excitons and biexcitons exhibit markedly disparate effective gap energies, electron-hole overlaps, and consequently, lifetimes.[27,28,44] In light of these considerations, the incorporation of the repulsive Coulomb potential and exchange-correlation terms into the Schrödinger equations for the case of MEG, which encompasses the presence of multiple electron-hole pairs within the QD structure, can facilitate the derivation of a more realistic effective gap energy and oscillator strength. In the case of MEG (biexciton), the Schrödinger equations can be expressed as follows:

$$\left[-\frac{\hbar^2}{2}\vec{\nabla}_r\left(\frac{1}{m_e^*(r,T,P)}\vec{\nabla}_r\right)+V_e(r,T,P)-q_e\Phi_h+q_e\Phi_e\right.$$
$$\left.+V_{xc}^{e-e}[\rho_e(r,T,P)]\right]R_e(r,T,P)=\varepsilon_e^{XX}(T,P)R_e^{XX}(r,T,P) \quad (8)$$

and

$$\left[-\frac{\hbar^2}{2}\vec{\nabla}_r\left(\frac{1}{m_h^*(r,T,P)}\vec{\nabla}_r\right)+V_h(r,T,P)-q_h\Phi_e+q_h\Phi_h\right.$$
$$\left.+V_{xc}^{h-h}[\rho_h(r,T,P)]\right]R_h(r,T,P)=\varepsilon_h^{XX}(T,P)R_h^{XX}(r,T,P) \quad (9)$$

The fourth terms of these equations represent the attractive Coulomb potential, while the fifth terms represent the exchange-correlation potentials between the same particles. Further details on this self-consistent calculation can be found in our previous works.[41,45]

As illustrated in Equations (8) and (9), the energy levels and wave functions in the biexciton state diverge from those in the exciton state. This discrepancy gives rise to a distinctive oscillator strength for the biexciton. The oscillator strength can be expressed in a revised form by employing the effective gap energy and wave functions for the biexcitonic state as follows:

$$f_{XX}=\frac{E_p}{2E_{gap}^{XX}}\left|\int\psi_e^{XX}(r)\psi_h^{XX}(r)d^3r\right|^2 \quad (10)$$

In our pervious study, we demonstrated that the bound/unbound states of quasi-particles, including positive trion, negative trion, and biexciton, which are localized in QDs, can have a significant impact on the recombination oscillator strength and lifetime.[28] In the bound biexciton state, the strong confinement effect causes all particles to move together when the QD size is small. In this case, each of the two electrons in the conduction band has the potential to recombine with the two holes in the valence band. The strong attractive Coulomb force exerted by the two holes on the electrons increases the probability of recombination. As the QD size increases, the unbound biexciton state is observed, with each exciton moving

independently within the structure. In this case, the recombination probability is expected to be half of that in the bound state. Considering the bound/unbound state, the oscillator strength parameter for the biexciton can be expressed as follows[28]:

$$f_{XX_2} = A\frac{E_p}{2E_{gap}^{XX}}\left|\int \psi_e^{XX}(r)\psi_h^{XX}(r)d^3r\right|^2 \tag{11}$$

Here, A is an integer value, set to 4 for a bound biexciton and 2 for an unbound biexciton.

2.2. Power Conversion Efficiency

The efficiency of a solar cell is defined as the ratio of the power produced by the cell to the total solar irradiance incident on it, P_{in}, which is standardized to an AM1.5 condition in the calculations. This efficiency can be computed using the following formula[46]:

$$\eta = \frac{J_{net}V}{P_{in}} \tag{12}$$

where V is the voltage applied to the cell, and J_{net} represents the net current density, which is the difference between the photogenerated current density, J_{pg}, and the recombination current density, J_{rc},

$$J_{net} = J_{pg} - J_{rc} \tag{13}$$

In the ODBM, the photogenerated current is calculated by taking into account the bandgap energy of the material used in the solar cell as follows[16,34,36]:

$$J_{pg} = q_e\int_{E_g}^{\infty} \mathrm{QY}(h\nu, E_g)\phi(h\nu)\, d(h\nu) \tag{14}$$

Here, q_e represents the electronic charge, ϕ denotes the solar photon flux density, and QY stands for the quantum yield of the absorbed photon, which is a function of the photon energy ($h\nu$) and the bandgap energy (E_g). The QY is equivalent to the external quantum efficiency (EQE), which measures the collection probability of the excited carriers ($C(h\nu)$), the reflectivity of the solar cell ($R(h\nu)$), and the absorptivity of the solar cell ($a(h\nu)$). This relationship can be expressed as [39]

$$\mathrm{EQE}(h\nu) = C(h\nu)(1 - R(h\nu))a(h\nu) \tag{15}$$

In the ODBM, to achieve maximum PCE, the ideal conditions assumed are that no photons are reflected, i.e., $R(h\nu) = 0$, and all photons with energy higher than the bandgap energy are absorbed, i.e., $a(h\nu) = 1$. As shown in Equation (15), under these ideal conditions, the EQE($h\nu$) and QY($h\nu, E_g$) are determined solely by $C(h\nu)$.

MEG, which plays a pivotal role in the potential for high efficiency in QDSCs, is incorporated into PCE calculations through the QY term, as illustrated below[16]:

$$\mathrm{QY}(h\nu, E_g) = \sum_{n=1}^{M}\theta(h\nu, nE_g) \tag{16}$$

where $\theta(h\nu, nE_g)$ denotes the Heaviside step function, and M is an integer given by $M = \frac{h\nu_{\max}}{E_g}$. Upon examination of the formula, it becomes evident that MEG occurs when the energy of the absorbed photon is in multiples of the bandgap energy, i.e., $\mathrm{QY}(h\nu, E_g) > 1$.

In ODBM, under ideal conditions, recombination of excited charges remains the only loss mechanism, which determines the recombination current density as follows[16,46]:

$$J_{rc} = \frac{2\pi q_e}{h^3c^2}\int_{E_g}^{\infty}\frac{\mathrm{QY}(h\nu, E_g)(h\nu)^2}{e^{(h\nu - q_eV\mathrm{QY}(h\nu,E_g))/kT} - 1}\, d(h\nu) \tag{17}$$

Here, h denotes Planck's constant, c represents the speed of light, k stands for Boltzmann's constant and T is temperature. The value of V is the voltage that maximizes the PCE of the solar cell and is determined through numerical search. Since emission is a component of the recombination current density, the emissivity, $\epsilon(h\nu)$, is replaced by the absorptivity in the EQE($h\nu$) formula as follows[39]

$$\mathrm{EQE}(h\nu) = C(h\nu)(1 - R(h\nu))\epsilon(h\nu) \tag{18}$$

The fundamental distinction between MDBM and ODBM lies in the incorporation of the oscillator strength parameter, which can unambiguously elucidate the response of confined quasiparticles in QD structures to any internal or external effects. This is achieved by incorporating the oscillator strength parameter into the collection probability, that is, $C(h\nu) = f\mathrm{QY}(h\nu)$. In MDBM, with this integration the recombination current density can be expressed as follows[39]:

$$J_{rc} = \frac{2\pi q_e}{h^3c^2}\int_{E_g}^{\infty}\frac{f\mathrm{QY}(h\nu, E_g)(h\nu)^2}{e^{(h\nu - fq_eV\mathrm{QY}(h\nu,E_g))/kT} - 1}\, d(h\nu) \tag{19}$$

The oscillator strength in QDs is derived from the wave functions of confined electrons and holes. These wave functions are influenced by factors such as confinement potential, confinement regime, and the effective masses of the electrons and holes. As a result, the oscillator strength parameter can vary significantly even in QDs with the same gap energy. Consequently, the MDBM approach may yield results for PCE calculations in QDSCs that are markedly different from those obtained using the ODBM approach.

3. Results and Discussion

In this study, a spherical CdSe/CdTe/ZnTe QD structure exhibiting a type-II confinement regime has been selected as a model structure. As seen in **Figure 1**, in this structure, the electron is confined in the CdSe core while the hole is confined in the ZnTe outer shell, and the CdTe spacer material is used as a precise tool for tuning the electron–hole wave function overlap. To obtain more realistic results, the quantum dot is assumed to be embedded in a glass matrix. Throughout all calculations, atomic units are employed, with the charge, electron bare mass, and Planck constant set to unity, i.e., $m_0 = e = \hbar = 1$. Additionally, the dielectric mismatch, which can critically affect the electronic and optical properties of the quantum dot, is also taken into account in

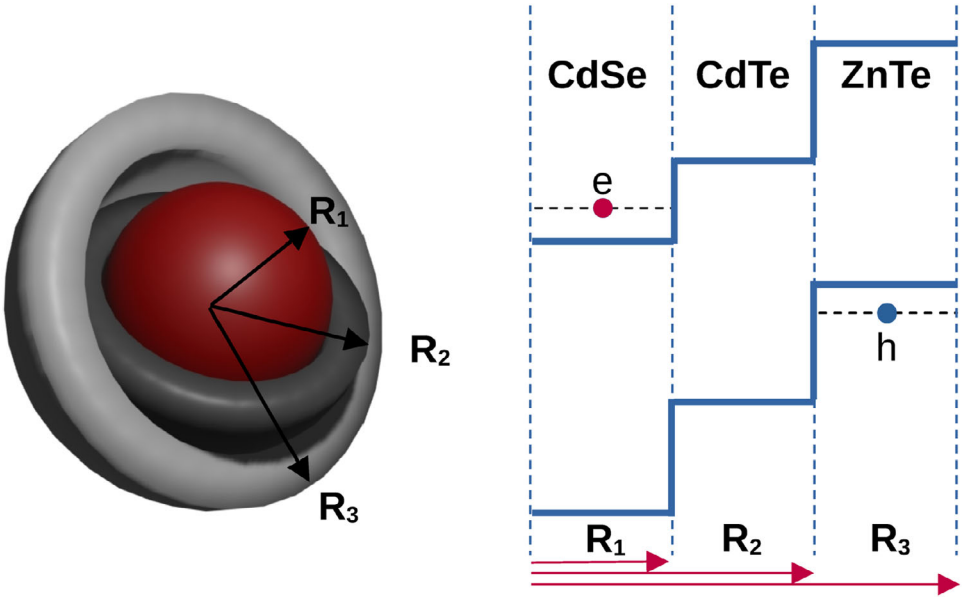

Figure 1. A schematic representation of a CdSe/CdTe/ZnTe quantum dot structure. In this structure, the electron is confined in the CdSe core, while the hole is confined in the ZnTe outer shell.

the calculations. All parameters used in the calculations are provided in the **Table 1**.

The study has examined the PCE in relation to core radius, CdTe and ZnTe layer thicknesses, temperature, and pressure parameters. The PCE has been evaluated under both the MDBM and the ODBM, with and without MEG. In the case of MEG, distinct PCE calculations have been conducted for both the excitonic gap energy and the biexcitonic gap energy (equivalent to one-half of the total biexciton energy). Moreover, the MEG scenario has been analyzed under three distinct conditions in calculations involving the MDBM. The aforementioned conditions are as follows:

- In Case 1, the single exciton wave functions have been employed in MEG calculations. This approach excludes the additional repulsive Coulomb term, as well as exchange-correlation effects caused by multiple excitons. In this case, the oscillator strength provided in Equation (1) has been utilized in the MDBM calculations.
- In Case 2, the biexciton wave functions have been employed for MEG calculations, including the repulsive and attractive Coulomb and exchange-correlation effects caused by multiple electron–hole pairs. In this case, the oscillator strength specified in Equation (10) has been used in the MDBM calculations.
- In Case 3, the biexciton bound/unbound states are additionally considered, thus building upon Condition 2. In this case, the oscillator strength outlined in Equation (11) has been employed in the MDBM calculations.

In the study, the CdSe/CdTe/ZnTe QD structure used as a model allows a maximum of 2 electrons in the ground state energy level. Therefore, for the with MEG case, the QY value is set to QY($h\nu$, E_g) = 2. The default values have been established as follows: the radius of the CdSe core is set at 1 nm, while the thicknesses of the CdTe and ZnTe shells are both fixed at 1 nm, temperature, T = 273 K (T = 0 °C), and pressure, P = 0 GPa. When analyzing the effects of a specific parameter, all other parameters have been held constant at their default values. For instance, when examining the influence of the CdSe core radius, the CdTe and ZnTe shell thicknesses have been kept at 1 nm, while temperature and pressure have been fixed at T = 273 K and P = 0 GPa, respectively.

It is well established that in a biexciton, which is composed of two electrons and two holes, the repulsive Coulomb interactions and exchange-correlation potentials between like charges result in the energy levels and wave functions of each exciton being distinct from those of a single exciton. This is despite both the single exciton and biexciton being subject to the same internal and external influences. As illustrated in the left panel of **Figure 2**, the PCE calculations utilizing ODBM for the MEG case demonstrate a notable decline in efficiency as the excitonic gap energy on the

Table 1. The material parameters used in the calculations.

	$m_h^*(0)$	$\kappa(0)$	$E_g(0)$ [eV]	E_P [eV]	Δ_0 [meV]	α [meV K^{-1}]	β [K]	a [meV GPa^{-1}]	b [meV GPa^{-2}]
CdSe	0.57[42]	9.60[42]	1.766[42]	21.0[47]	410[42]	0.696[42]	281[42]	−15[42]	—
CdTe	0.82[42]	10.40[42]	1.600[42]	20.7[48]	900[42]	0.5[42]	180[42]	84[42]	−3.96[42]
ZnTe	0.67[42]	9.40[42]	2.383[42]	19.1[49]	950[42]	0.549[42]	159[42]	103[42]	−2.4[42]

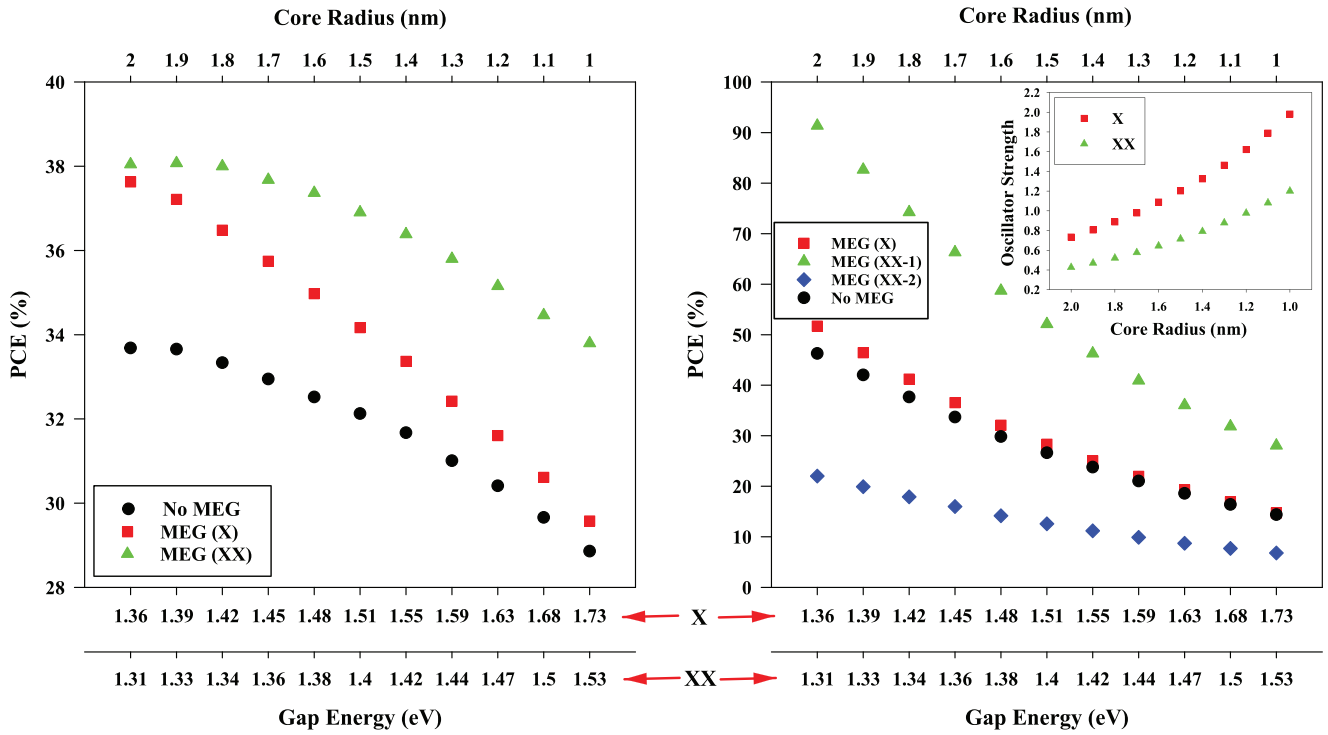

Figure 2. The variation of the PCE with CdSe core radius is presented, with the results of calculations made using ODBM (left panel) and MDBM (right panel) shown. The top axes represent the change in CdSe core radius, while the bottom axes correspond to the excitonic effective gap energy levels for each core radius. The bottom offset axis displays the biexcitonic effective gap energy, which is calculated by including all biexcitonic effects such as attractive and repulsive Coulomb potentials and exchange-correlation effects for each core radius. The inset of the left panel shows the variation of exciton and biexciton oscillator strength with the core radius. Here, the CdTe and ZnTe layer thicknesses have been fixed at 1 nm.

bottom axis increases from 1.36 to 1.73 eV. This is evidenced by a reduction in the PCE from approximately 38–30% (red squares). In contrast, calculations utilising the biexcitonic effective gap energy, as observed on the bottom offset axis, illustrate an increase in effective gap energy from 1.31 to 1.53 eV, accompanied by a decrease in PCE from approximately 38% to 34% (green triangles). Upon close examination, it becomes evident that the biexcitonic effective gap energy remains lower than the excitonic effective gap energy. This suggests the existence of a bound biexciton. The small size of the QD and the influence of the confinement potential result in the two electrons and two holes forming the biexciton being forced to stay together. Consequently, the attractive Coulomb potential between different charges prevails over the repulsive Coulomb potential between like charges, thereby leading to the formation of a bound biexciton. As the radius of the CdSe core increases to 2 nm, the spatial distance between the electrons and holes increases, thereby balancing the attractive and repulsive Coulomb potentials. Consequently, the excitonic effective gap energy (1.36 eV) and the biexcitonic effective gap energy (1.31 eV) become nearly equal. This balance results in the PCE being almost equal in the ODBM calculations when the CdSe core radius is 2 nm. The results unambiguously illustrate that there is a discernible discrepancy between the PCE calculations conducted with the excitonic effective gap energy and those performed with the biexcitonic effective gap energy when the MEG case is taken into account. This discrepancy underscores the necessity of incorporating the biexcitonic effective gap energy into such calculations. In the case of the without MEG, as anticipated, the reduction in the CdSe core radius from 2 to 1 nm resulted in a decline in the PCE, from approximately 34% to 29%.

The right panel of Figure 2 illustrates the variation of PCE with the CdSe core radius, as calculated using MDBM. The bottom axis, analogous to the left panel, represents the excitonic gap energy for each core radius, while the bottom offset axis depicts the biexcitonic gap energy for the same core radius. As MDBM considers oscillator strength in addition to gap energy, the resulting calculations differ from those obtained using ODBM. As demonstrated in Equations (1), (10), and (11), oscillator strength is calculated in three distinct ways. The curve designated as MEG (X) in the figure represents the PCE calculation employing excitonic gap energy and wavefunctions in the MEG case. As illustrated in the figure, the PCE exhibits a notable decline from approximately 52% to around 18% with the reduction in the CdSe core radius. In the ODBM calculations, where only the excitonic gap energy was considered, the PCE exhibited a decrease from approximately 38% to around 30% with the reduction in core radius. This indicates the critical impact of oscillator strength on the PCE. As shown in the inset of the right panel (red square), the change in oscillator strength with decreasing CdSe core radius reveals that the oscillator strength increases to around 2, as expected. With increasing oscillator strength, the recombination probability of the charges increases, leading to a significant decrease in PCE by reducing the collection probability and recombination current density, as predicted by MDBM. In the case of

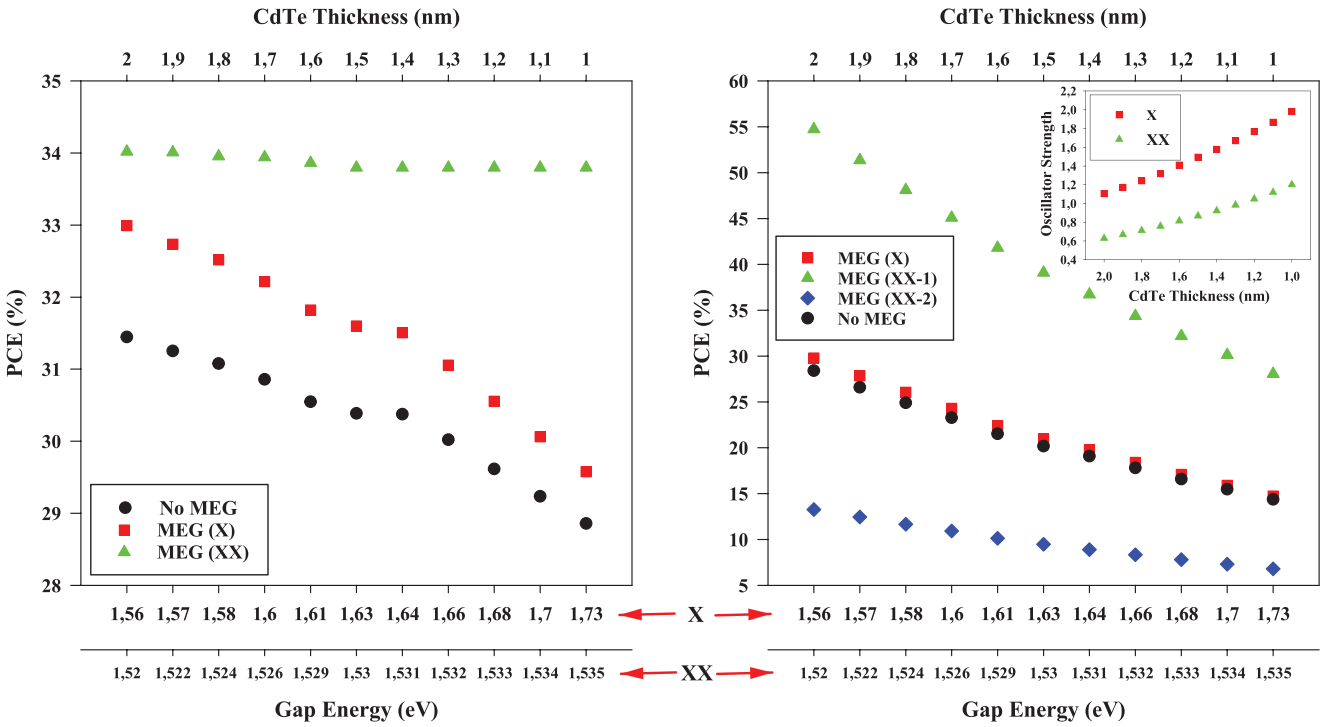

Figure 3. Variation of the PCE with CdTe layer size (top axis) calculated using ODBM (left panel) and MDBM (right panel). The exciton effective gap energy calculated for each CdTe size is shown on the bottom axis, and the biexciton effective gap energy is displayed on the bottom offset axis. The excitonic and biexcitonic oscillator strength values are presented in the inset of the right panel. Here, the CdSe core radius and ZnTe layer thickness have been fixed at 1 nm.

MEG (XX-1), when both of the biexcitonic energy levels and wavefunctions are taken into account, the PCE value exceeds 90% for a CdSe core radius of 2 nm (green triangles). This remarkably high PCE value rapidly declines to approximately 30% as the CdSe core radius is reduced to 1 nm. This suggests that oscillator strength exerts a considerable influence. As illustrated in the inset of the right panel, the oscillator strength in the biexcitonic case is less than that in the excitonic case. Consequently, the recombination probability is reduced, which has a positive impact on the PCE.

In the calculations made with oscillator strength, which also takes into account the biexciton bound state given in Equation (11), the PCE is markedly lower than in all other cases, as evidenced in the right panel of Figure 2 (blue diamonds). In all calculations conducted throughout this study, a bound biexcitonic state was consistently obtained, resulting in the A value in Equation (11) being set to 4 in all cases. This fourfold increase in oscillator strength markedly elevates the recombination probability, and, consequently, the recombination current density to a greater extent than in other cases. As a consequence of these factors, the PCE declines from approximately 23% to around 8% as the CdSe core radius is reduced from 2 to 1 nm. Given that the highest recorded efficiency for current quantum dot solar cells (QDSCs) is approximately 19%, one of the underlying reasons may be the significantly different recombination probabilities observed in quantum dot structures. In the absence of MEG, the PCE declines from approximately 48% to around 18% as the core radius diminishes from 2 to 1 nm (black sphere). One of the most intriguing outcomes of this study is that in the absence of MEG, the PCE attains higher values compared to the presence of MEG, which considers the biexciton bound state.

In the CdSe/CdTe/ZnTe QD structure, no particles are confined within the CdTe layer. Therefore, in this structure, CdTe can be employed as a tuning tool for electron–hole wavefunction overlap, through the implementation of minimal alterations to the energy of the electron and hole. The left panel of the **Figure 3**, illustrates the impact of varying the thickness of the CdTe layer on the change in PCE using ODBM. As the thickness of the CdTe layer is reduced from 2 to 1 nm (as indicated on the top axis), the excitonic gap energy increases from 1.56 to 1.73 eV. Conversely, the biexcitonic energy level rises from 1.52 to 1.535 eV, exhibiting an almost imperceptible change (the bottom offset axis). Although no charge is localized in the CdTe layer, the reason behind the change in the excitonic gap energy with varying layer thickness is the small radius of the CdSe core (1 nm). Due to the high energy of the electron, it penetrates into the CdTe layer and responds to the variation in layer size to some extent. In the case of the biexcitonic gap energy, as the thickness of the CdTe layer increases, the spatial distance between the electron and hole increases, resulting in a decrease in the attractive Coulomb force. However, since the radius of the CdSe core and the thickness of the ZnTe layer remain constant, the repulsive Coulomb force between the same particles becomes dominant, compensating for the loss in biexcitonic gap energy. Upon examination of the change in the PCE for the with MEG case, it was observed that the PCE calculated with excitonic gap energy decreased from approximately 33% to around 30%. Conversely, the PCE calculation conducted with biexcitonic gap energy reveals that the PCE

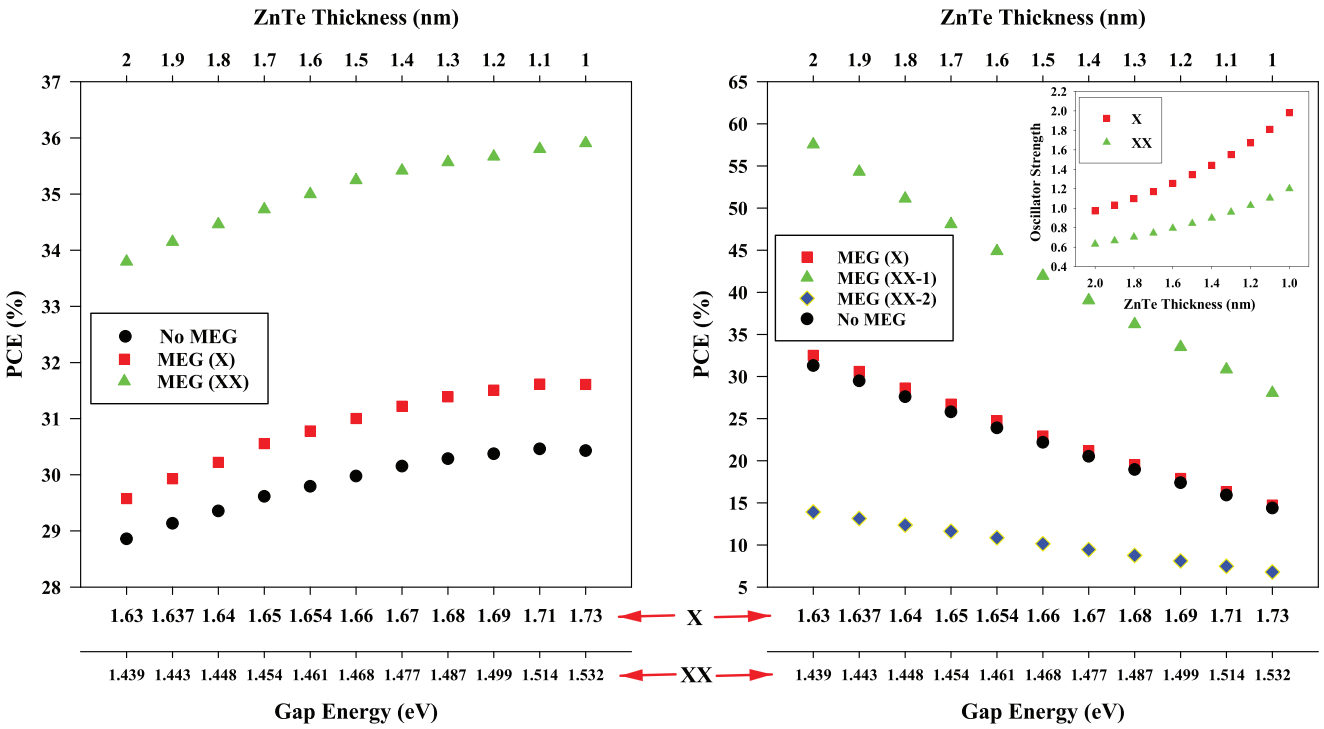

Figure 4. In contrast to the variations illustrated in Figures 2 and 3, the variations shown here are dependent on the thickness of the ZnTe layer. The radius of the CdSe core and the thickness of the CdTe layer have both been set to 1 nm.

remains largely unaltered, thereby maintaining a consistent PCE of approximately 34%. This demonstrates that the change in CdTe layer thickness exerts a negligible influence on the PCE. This is an anticipated outcome in ODBM, which solely considers the gap energy. In the absence of MEG, as anticipated, the PCE assumes lower values, declining from 31.5% to 29%. The excitonic gap energy in both the with MEG and without MEG cases converges as the gap energy increases. This is due to the reduction in the flux of high-energy photons reaching the Earth.

The right panel of the Figure 3 illustrates the PCE calculated using MDBM as a function of the CdTe layer thickness. It can be observed that as the CdTe layer thickness decreases, the oscillator strength increases (as demonstrated in the inset of the right panel), resulting in a decline in PCE across both the with and without MEG scenarios. While the biexcitonic energy level remains relatively unaltered, the oscillator strength in the biexcitonic case exhibits an increase from approximately 0.6 to around 1.2 as the CdTe layer thickness decreases (illustrated by the green triangles in the inset). This increase in oscillator strength contributes to the observed reduction in PCE from 55% to 29%. In the excitonic case, both the gap energy and oscillator strength increase as the CdTe layer thickness decreases. The oscillator strength is nearly twice as high as in the biexcitonic case (as shown in the inset). Consequently, a reduction in the CdTe layer thickness from 2 nm to 1 nm results in a notable decline in PCE, from approximately 30% to approximately 15%. In considering the biexciton bound state, it is observed that the oscillator strength increases fourfold across all layer thicknesses due to the formation of bound biexcitons, which leads to a further reduction in PCE. Specifically, as the CdTe layer thickness is reduced, the PCE declines from approximately 14% to around 6%. In the absence of MEG, the PCE is approximately 2% lower at higher CdTe layer thicknesses compared to the excitonic with MEG case. However, as the CdTe layer thickness is decreased, the PCE in the absence of MEG approaches that of the excitonic with MEG case.

Due to their higher effective masses, holes are observed to have a lower energy state. Consequently, the energy changes of holes with the variation in the thickness of the layer in which they are localized are significantly smaller in comparison to those of electrons in a QD structure. The left panel of **Figure 4** depicts the outcomes of PCE alterations calculated with ODBM for the ZnTe layer thickness in the CdSe/CdTe/ZnTe QD structure, wherein the holes are confined. As illustrated on the bottom axes, the excitonic gap energy increases from 1.63 to 1.73 eV as the thickness of the ZnTe layer decreases from 2 to 1 nm, indicating a 100 meV increase. The biexcitonic gap energy increases from 1.439 to 1.532 eV for the same change in layer thickness (bottom offset axis), indicating a 93 meV increase. A comparison of the aforementioned gap energy changes with those resulting from variations in the CdTe layer thickness reveals that while the excitonic gap energy exhibits a comparatively minor alteration, the biexcitonic energy level demonstrates a more pronounced change. As previously stated, the high energy of the electron allows it to penetrate the CdTe layer, resulting in a greater-than-expected impact on the excitonic gap energy due to the size variation of this layer. However, in the case of variations in the thickness of the ZnTe layer, the electron is almost unaffected by this change in size. Moreover, the relatively minor energy change of the low-energy hole due to ZnTe layer thickness results in a more limited excitonic gap energy change compared to the excitonic gap energy change due to

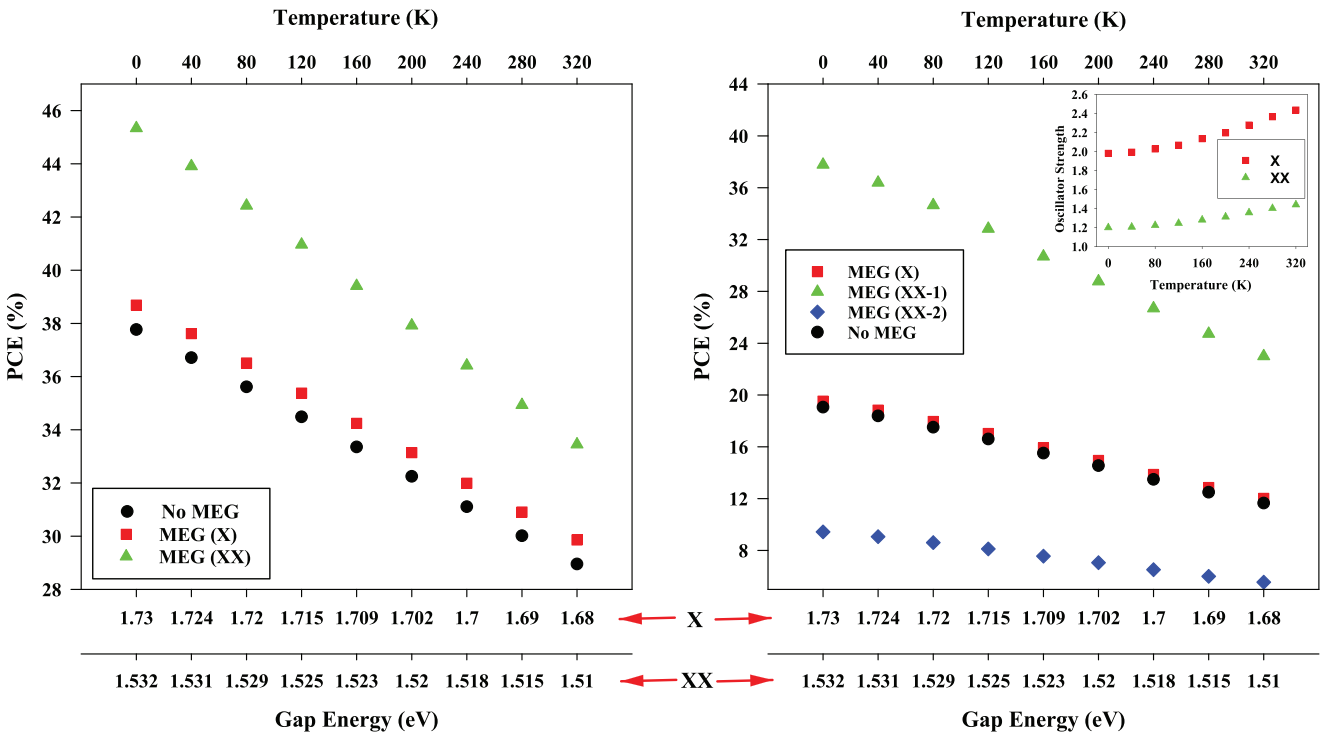

Figure 5. Temperature-dependent variation of PCE calculated using ODBM (left panel) and MDBM (right panel). The bottom axes represent the excitonic gap energy at each temperature, while the bottom offset axes display the biexcitonic gap energy at the same temperatures. The inset in the right panel shows the temperature-dependent changes in oscillator strength for excitons and biexcitons.

CdTe layer variations. In the biexcitonic case, as the thickness of the ZnTe layer increases, the energy of the holes decreases and the distance between the holes increases, thereby reducing the repulsive Coulomb potential. Consequently, the biexcitonic gap energy decreases. A reduction in excitonic gap energy results in a decline in PCE, from approximately 31.5% to around 29.5% in the MEG case and from around 30% to just below 29% in the absence of MEG, as the thickness of the ZnTe layer decreases. In calculations conducted with the biexcitonic gap energy, the PCE was observed to decrease from approximately 36% to around 34% as the ZnTe thickness increased. This suggests that in calculations made with ODBM, the repulsive Coulomb interaction may have a significant impact on the PCE.

Upon examination of the results obtained with MDBM for the PCE's dependence on ZnTe layer thickness, as illustrated in the right panel of Figure 4, a comparable trend to the alterations in CdTe layer thickness is observed at low ZnTe layer thicknesses. However, at higher ZnTe layer thicknesses, the repulsive Coulomb potential between holes diminishes, resulting in diminished oscillator strength values in comparison to the changes in CdTe layer thickness. Consequently, the PCE reaches higher values.

In QD structures, the electronic and optical properties are influenced by intrinsic factors, such as the material type and size, as well as external factors, including temperature and pressure. A comprehensive understanding of the response of QD structures to temperature is of paramount importance for the successful design of QDSCs. **Figure 5** presents a comparison of the temperature dependence of PCE in CdSe/CdTe/ZnTe QDSCs, utilizing both ODBM and MDBM. As illustrated in the left panel, the ODBM calculations indicate that the PCE decreases with temperature across all scenarios examined. As seen in **Figure 6** (top panels), it is observed that the bulk gap energy and the effective masses of electrons and holes are observed to decrease with increasing temperature. While the kinetic energies of electrons and holes exhibit a slight increase due to the reduction in their effective masses, the decline in gap energy results in a decrease in effective gap energy in both excitonic and biexcitonic states as temperature increases (bottom axes). In the biexcitonic state, the twofold increase in kinetic energy for the two electrons and two holes results in a slight reduction in effective gap energy compared to the excitonic state. As the temperature increases, the PCE values demonstrate a notable decrease in the excitonic MEG case, with a 9% increase observed when the temperature is elevated from 4 to 320 K. In the biexcitonic state, the decrease is approximately 12%. In the without MEG case, which also employs the excitonic effective gap energy, the PCE exhibits a 9% rise with increasing temperature.

The right panel of Figure 5 illustrates the temperature dependence of PCE calculated using MDBM. The MDBM calculations indicate a reduction in PCE with increasing temperature across all cases. This phenomenon can be attributed to the observed increase in oscillator strength with temperature, as illustrated in the inset of the figure. As the temperature increases, the bulk gap energy decreases, leading to a reduction in the confinement potential for electrons and holes. This reduction in confinement potential results in the movement of electrons and holes closer together, due to their attractive Coulomb interaction.

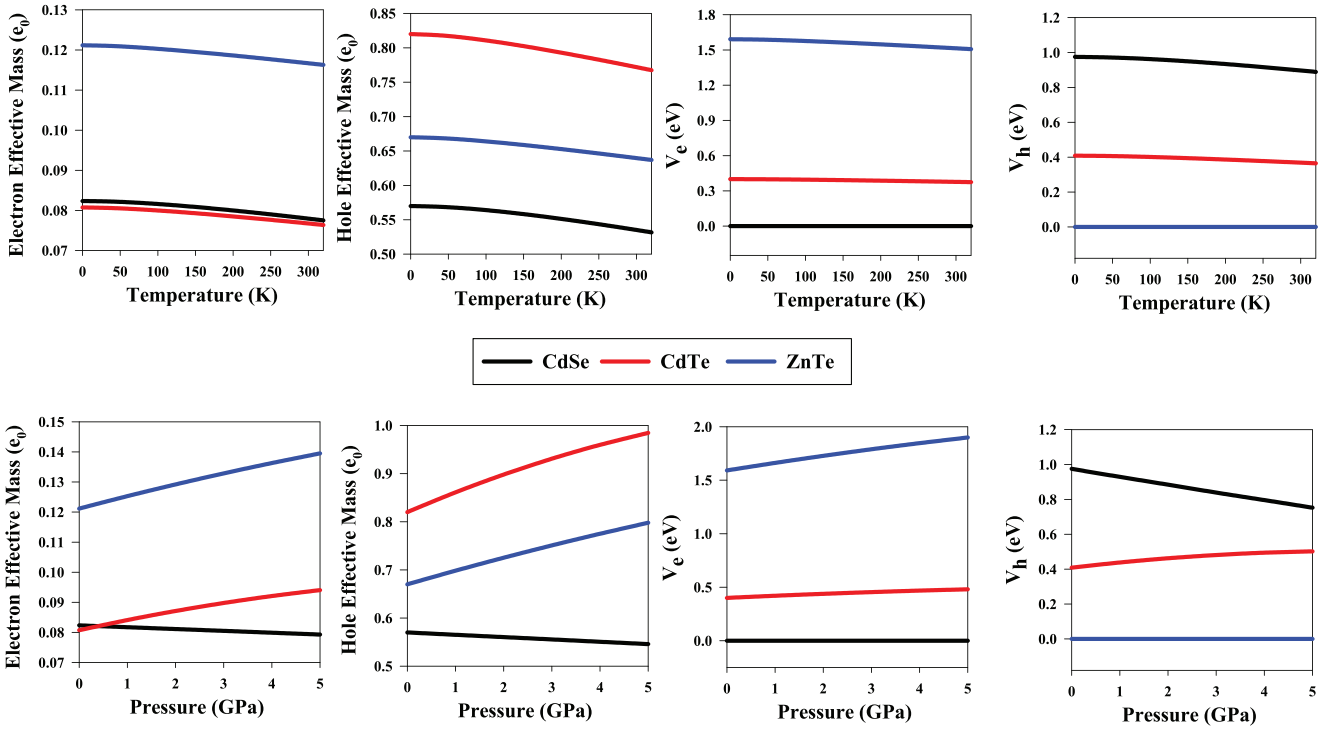

Figure 6. From left to right, the figure shows the variation of the electron's effective mass, hole's effective mass, electron's confinement potential, and hole's confinement potential as a function of temperature (top graphs) and hydrostatic pressure (bottom graphs).

Furthermore, the increase in the kinetic energy of electrons and holes, attributable to their diminished effective masses at elevated temperatures, facilitates their easier penetration of the confinement potential. Consequently, the overlap of electron–hole wave functions increases, resulting in higher oscillator strength. In the biexcitonic case, the oscillator strength is lower than in the excitonic case, resulting in the highest PCE values observed for biexcitonic scenarios. In considering the biexciton bound state, the presence of bound biexcitons at all temperatures results in a fourfold increase in oscillator strength, which in turn yields the lowest PCE values. In the excitonic state, both with and without MEG, the PCE values are nearly identical. This is due to the fact that the excitonic effective gap energy shifts into an energy range where the impact of MEG is significantly reduced. A review of the literature reveals that experimental studies have demonstrated a negative impact of elevated temperatures on the PCE of QDSCs.[50,51] In this regard, the temperature-dependent results obtained from both ODBM and MDBM are found to be consistent with the experimental observations. However, in MDBM, an increase in temperature results in a further decrease in PCE due to the effect of oscillator strength.

Figure 7 depicts the impact of hydrostatic pressure on the PCE of CdSe/CdTe/ZnTe QDSCs. As illustrated in the bottom axes of the figure, both the excitonic and biexcitonic gap energies demonstrate an increase with increasing pressure. This finding is consistent with the trends observed in Figure 6 (bottom panels), which illustrate that the effective mass of the electron in CdSe decreases with increasing pressure, leading to an increase in the energy of the electron. Furthermore, the bulk gap energy also exhibits an increase under pressure. While the effective mass of the hole in ZnTe increases, leading to a decrease in its energy, the overall increase in electron energy and bulk gap energy results in an increase in both excitonic and biexcitonic gap energies with increasing pressure. The repulsive Coulomb interaction between like charges results in a less pronounced increase in the biexcitonic gap energy compared to the excitonic gap energy. The effective gap energies are situated within the high-energy spectrum. As these high-energy photons reach Earth in lower intensities, the shift to an even higher energy spectrum with increasing pressure results in a decrease in PCE across all cases in ODBM, as illustrated in the left panel of the figure. In particular, the biexcitonic scenario demonstrates a decrease in PCE of approximately 2%, while both the excitonic scenarios with and without MEG exhibit a decrease of approximately 4% in PCE with increasing pressure.

In contrast, PCE calculations performed with the MDBM indicate an elevated PCE with increasing pressure. This increase can be attributed to the enhanced bulk gap energy under pressure, which leads to an increase in the confinement potential experienced by both electrons and holes. The enhanced confinement results in a reduction of the overlap between the electron and hole wave functions, which in turn leads to a decrease in oscillator strength, as illustrated in the inset of the right panel. The reduction in oscillator strength thus results in an increase in PCE. This effect is particularly pronounced in the biexcitonic case, where the increase in PCE is more significant compared to the excitonic scenario. Moreover, the increase in hole effective mass under pressure results in a further reduction in hole mobility, leading to an even greater decline in oscillator strength in comparison to the excitonic case. Consequently, the PCE attains

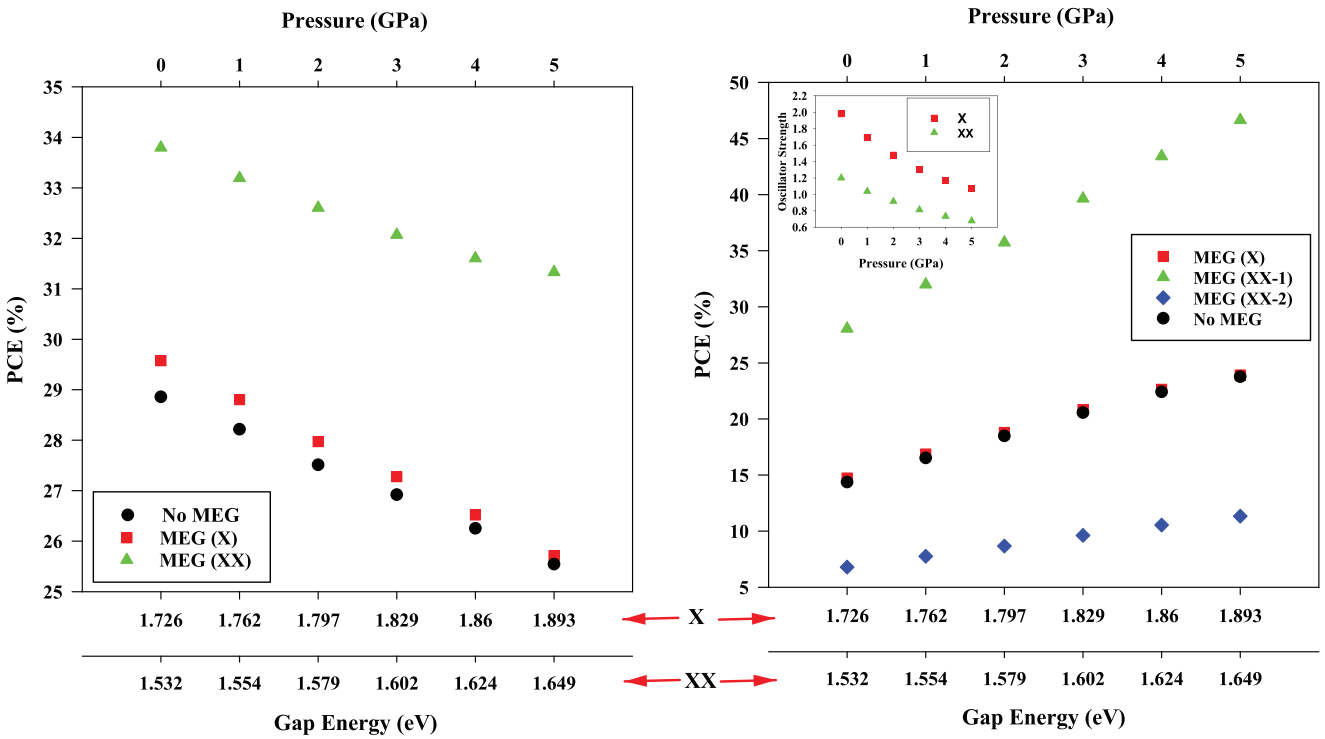

Figure 7. The figure format is identical to that of Figure 5. This figure illustrates the variation in the data set with respect to hydrostatic pressure.

elevated values in the biexcitonic scenario. In the case of excitonic effects, the PCE values for both scenarios with and without MEG remain largely unaltered as pressure increases. This is due to the fact that the high excitonic effective gap energy results in a reduction of the MEG effect, which in turn brings the PCE closer to that of the scenario without MEG. In the approach that considers the bound biexciton state, the presence of bound biexcitons is observed at all pressure levels. As illustrated in the figure, the oscillator strength is fourfold due to the bound biexciton, resulting in markedly lower PCE values compared to other scenarios. A similar trend is observed with increasing pressure, as seen in the PCE calculations using ODBM and MDBM. While ODBM calculations indicate a decline in PCE with rising pressure, MDBM calculations demonstrate an enhancement in PCE under the same conditions.

4. Conclusion

In conclusion, the strong confinement effects in QD structures, which induce distinctly different quantum phenomena in excitons and biexcitons, significantly modify their electronic and optical properties, thereby critically affecting the PCE of QDSCs. A notable discrepancy has been identified between the PCE calculations conducted with the excitonic effective gap energy and those with the biexcitonic effective gap energy, across both the ODBM and MDBM models. Furthermore, calculations utilizing the MDBM model indicate that the biexciton bound state, which affects the biexciton recombination mechanism, exerts a considerable influence on the PCE through its impact on the recombination current density. The strong Coulomb attraction between the two electrons and two holes forming the bound biexciton results in a fourfold increase in the oscillator strength, which leads to a significant reduction in the PCE. While PCE calculations based on excitonic and biexcitonic effective gap energies in the presence of MEG can yield very high PCE values, the inclusion of the biexciton bound state limits the PCE to approximately 20%, which is in agreement with the current maximum values for PCE in QDSCs. Moreover, the study demonstrates that core radius, shell thickness, temperature, and pressure markedly influence the PCE, underscoring the pivotal role of these parameters in QDSC design. This research offers crucial insights into QDSCs and will likely inform efforts to attain higher PCE values in practical applications.

Conflict of Interest

The authors declare no conflict of interest.

Data Availability Statement

The data that support the findings of this study are available from the corresponding author upon reasonable request.

Keywords

biexciton bound state, detailed balance model, excitonic and biexcitonic gap energy, quantum dot solar cells

Received: September 3, 2024
Revised: November 15, 2024
Published online: December 3, 2024

[1] J. Tian, G. Cao, *Nano Rev.* **2013**, *4*, 22578.
[2] A. J. Nozik, *Phys. E* **2002**, *14*, 115.
[3] R. P. Raffaelle, S. L. Castro, A. F. Hepp, S. G. Bailey, *Prog. Photovoltaics* **2002**, *10*, 433.
[4] A. J. Nozik, M. C. Beard, J. M. Luther, M. Law, R. J. Ellingson, J. C. Johnson, *Chem. Rev.* **2010**, *110*, 6873.
[5] D. J. Binks, *Phys. Chem. Chem. Phys.* **2011**, *13*, 12693.
[6] C. Smith, D. Binks, *Nanomaterials* **2013**, *4*, 19.
[7] A. Shabaev, A. L. Efros, A. J. Nozik, *Nano Lett.* **2006**, *6*, 2856.
[8] W. Shockley, H. J. Queisser, *J. Appl. Phys.* **1961**, *32*, 510.
[9] D. He, M. Zeng, Z. Zhang, Y. Bai, G. Xing, H.-M. Cheng, Y. Lin, *Smart Mat.* **2023**, *4*, e1176.
[10] Y. Liu, H. Wu, G. Shi, Y. Li, Y. Gao, S. Fang, H. Tang, W. Chen, T. Ma, I. Khan, K. Wang, C. Wang, X. Li, Q. Shen, Z. Liu, W. Ma, *Adv. Mater.* **2023**, *35*, 2207293.
[11] H. Song, H. Mu, J. Yuan, B. Liu, G. Bai, S. Lin, *SusMat* **2023**, *3*, 543.
[12] M. Wang, S. Liu, A. Wei, T. Luo, X. Wen, M.-Y. Li, H. Lu, *ACS Appl. Mater. Interfaces* **2024**, *16*, 24572.
[13] T. Xiao, S. Tu, T. Tian, W. Chen, W. Cao, S. Liang, R. Guo, L. Liu, Y. Li, T. Guan, H. Liu, K. Wang, M. Schwartzkopf, R. A. Fischer, S. V. Roth, P. Müller-Buschbaum, *Nano Energy* **2024**, *125*, 109555.
[14] M. Li, Y. Bao, W. Hui, K. Sun, L. Gu, X. Kang, D. Wang, B. Wang, H. Deng, R. Guo, Z. Li, X. Jiang, P. Müller-Buschbaum, L. Song, W. Huang, *Adv. Mater.* **2024**, *36*, 2309890.
[15] A. Polman, H. A. Atwater, *Nat. Mater.* **2012**, *11*, 174.
[16] M. Hanna, A. Nozik, *J. Appl. Phys.* **2006**, *100*, 7.
[17] U. Bockelmann, T. Egeler, *Phys. Rev. B* **1992**, *46*, 15574.
[18] C. T. Smith, E. J. Tyrrell, M. A. Leontiadou, J. Miloszewski, T. Walsh, M. Cadirci, R. Page, D. Binks, S. Tomić, *Sol. Energy Mater. Sol. Cells* **2016**, *158*, 160.
[19] https://www.nrel.gov/pv/cell-efficiency.html, (accessed: August, 2024).
[20] A. M. Dennis, B. D. Mangum, A. Piryatinski, Y.-S. Park, D. C. Hannah, J. L. Casson, D. J. Williams, R. D. Schaller, H. Htoon, J. A. Hollingsworth, *Nano Lett.* **2012**, *12*, 5545.
[21] A. Emre Kavruk, M. Sahin, F. Koc, *J. Appl. Phys.* **2013**, *114*, 18.
[22] A. E. Kavruk, *Philos. Mag.* **2018**, *98*, 3109.
[23] F. Koç, A. E. Kavruk, M. Sahin, *Phys. E* **2023**, *145*, 115479.
[24] F. Koç, *Eur. Phys. J. Plus* **2023**, *138*, 1124.
[25] A. Bracker, E. Stinaff, D. Gammon, M. Ware, J. Tischler, D. Park, D. Gershoni, A. Filinov, M. Bonitz, F. Peeters, et al., *Phys. Rev. B: Condens. Matter Mater. Phys.* **2005**, *72*, 035332.
[26] G. A. Narvaez, G. Bester, A. Zunger, *Phys. Rev. B: Condens. Matter Mater. Phys.* **2005**, *72*, 245318.
[27] K. Cho, T. Sato, T. Yamada, R. Sato, M. Saruyama, T. Teranishi, H. Suzuura, Y. Kanemitsu, *ACS nano* **2024**, *18*, 5723.
[28] M. Sahin, F. Koç, *Appl. Phys. Lett.* **2013**, *102*, 18.
[29] R. J. Ellingson, M. C. Beard, J. C. Johnson, P. Yu, O. I. Micic, A. J. Nozik, A. Shabaev, A. L. Efros, *Nano Lett.* **2005**, *5*, 865.
[30] J. Pijpers, E. Hendry, M. Milder, R. Fanciulli, J. Savolainen, J. Herek, D. Vanmaekelbergh, S. Ruhman, D. Mocatta, D. Oron, A. Aharoni, U. Banin, M. Bonn, *J. Phys. Chem. C* **2007**, *111*, 4146.
[31] M. C. Beard, K. P. Knutsen, P. Yu, J. M. Luther, Q. Song, W. K. Metzger, R. J. Ellingson, A. J. Nozik, *Nano Lett.* **2007**, *7*, 2506.
[32] Y. Kobayashi, T. Udagawa, N. Tamai, *Chem. Lett.* **2009**, *38*, 830.
[33] S. K. Stubbs, S. J. Hardman, D. M. Graham, B. F. Spencer, W. R. Flavell, P. Glarvey, O. Masala, N. L. Pickett, D. J. Binks, *Phys. Rev. B* **2010**, *81*, 081303.
[34] S. Tomić, J. M. Miloszewski, E. J. Tyrrell, D. J. Binks, *IEEE J. Photovoltaics* **2015**, *6*, 179.
[35] M. L. Boohm, T. C. Jellicoe, M. Tabachnyk, N. J. Davis, F. Wisnivesky-Rocca-Rivarola, C. Ducati, B. Ehrler, A. A. Bakulin, N. C. Greenham, *Nano Lett.* **2015**, *15*, 7987.
[36] M. A. Leontiadou, E. J. Tyrrell, C. T. Smith, D. Espinobarro-Velazquez, R. Page, J. Miloszewski, T. Walsh, D. Binks, S. Tomić, et al., *Sol. Energy Mater. Sol. Cells* **2017**, *159*, 657.
[37] M. C. Beard, *J. Phys. Chem. Lett.* **2011**, *2*, 1282.
[38] M. C. Beard, J. M. Luther, O. E. Semonin, A. J. Nozik, *Acc. Chem. Res.* **2013**, *46*, 1252.
[39] M. Sahin, *J. Phys.: Condens. Matter* **2018**, *30*, 205301.
[40] M. Şahin, S. Nizamoglu, A. E. Kavruk, H. V. Demir, *J. Appl. Phys.* **2009**, *106*, 4.
[41] F. Koc, M. Sahin, *J. Appl. Phys.* **2014**, *115*, 19.
[42] S. Adachi, *Properties of Semiconductor Alloys: Group-IV, III-V and II-VI Semiconductors*, John Wiley & Sons, Hoboken, NJ **2009**.
[43] M. Şahin, S. Nizamoglu, O. Yerli, H. Volkan Demir, *J. Appl. Phys.* **2012**, *111*, 2.
[44] M. E. Reimer, M. P. van Kouwen, A. W. Hidma, M. H. van Weert, E. P. Bakkers, L. P. Kouwenhoven, V. Zwiller, *Nano Lett.* **2011**, *11*, 645.
[45] A. Aktürk, M. Sahin, F. Koç, A. Erdinc, *J. Phys. D: Appl. Phys.* **2014**, *47*, 285301.
[46] R. Brendel, J. H. Werner, H. J. Queisser, *Sol. Energy Mater. Sol. Cells* **1996**, *41*, 419.
[47] E. W. Van Stryland, M. Woodall, H. Vanherzeele, M. Soileau, *Opt. Lett.* **1985**, *10*, 490.
[48] G. Wu, T. McGill, *J. Appl. Phys.* **1985**, *58*, 3914.
[49] Y. Rajakarunanayake, R. Miles, G. Wu, T. McGill, *Phys. Rev. B* **1988**, *37*, 10212.
[50] E. Garduno-Nolasco, M. Missous, D. Donoval, J. Kovac, M. Mikolasek, *J. Semicond.* **2014**, *35*, 054001.
[51] M. Xing, Y. Zhang, Q. Shen, R. Wang, *Sol. Energy* **2020**, *195*, 1.